ACS APPLIED MATERIALS & INTERFACES

Research Article

www.acsami.org

BMP-2 Derived Peptide and Dexamethasone Incorporated Mesoporous Silica Nanoparticles for Enhanced Osteogenic Differentiation of Bone Mesenchymal Stem Cells

Xiaojun Zhou,[†,‡] Wei Feng,[‡] Kexin Qiu,[†,‡] Liang Chen,[‡] Weizhong Wang,[‡] Wei Nie,[‡] Xiumei Mo,[†,‡] and Chuanglong He*[,†,‡]

[†]College of Chemistry, Chemical Engineering and Biotechnology; State Key Laboratory for Modification of Chemical Fibers and Polymer Materials, Donghua University, Shanghai 201620, China

[‡]College of Materials Science and Engineering, Donghua University, Shanghai 201620, China

Supporting Information

ABSTRACT: Bone morphogenetic protein-2 (BMP-2), a growth factor that induces osteoblast differentiation and promotes bone regeneration, has been extensively investigated in bone tissue engineering. The peptides of bioactive domains, corresponding to residues 73−92 of BMP-2 become an alternative to reduce adverse side effects caused by the use of high doses of BMP-2 protein. In this study, BMP-2 peptide functionalized mesoporous silica nanoparticles (MSNs-pep) were synthesized by covalently grafting BMP-2 peptide on the surface of nanoparticles via an aminosilane linker, and dexamethasone (DEX) was then loaded into the channel of MSNs to construct nanoparticulate osteogenic delivery systems (DEX@MSNs-pep). The in vitro cell viability of MSNs-pep was tested with bone mesenchymal stem cells (BMSCs) exposure to different particle concentrations, revealing that the functionalized MSNs had better cytocompatibility than their bare counterparts, and the cellular uptake efficiency of MSNs-pep was remarkably larger than that of bare MSNs. The in vitro results also show that the MSNs-pep promoted osteogenic differentiation of BMSCs in terms of the levels of alkaline phosphatase (ALP) activity, calcium deposition, and expression of bone-related protein. Moreover, the osteogenic differentiation of BMSCs can be further enhanced by incorporating of DEX into MSNs-pep. After intramuscular implantation in rats for 3 weeks, the computed tomography (CT) images and histological examination indicate that this nanoparticulate osteogenic delivery system induces effective osteoblast differentiation and bone regeneration in vivo. Collectively, the BMP-2 peptide and DEX incorporated MSNs can act synergistically to enhance osteogenic differentiation of BMSCs, which have potential applications in bone tissue engineering.

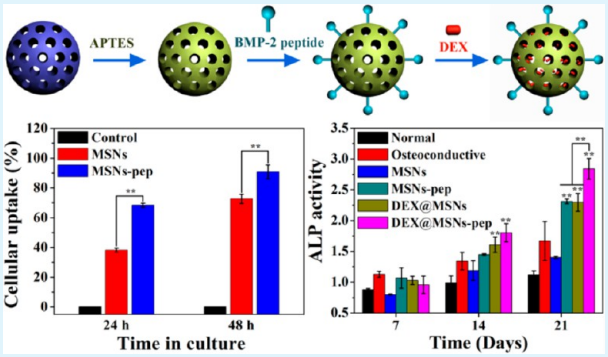

KEYWORDS: *mesoporous silica nanoparticles, dexamethasone, bone morphogenetic peptide, cellular uptake, osteogenic differentiation*

1. INTRODUCTION

Currently, autografts and allografts are the main modalities for the treatment of bone defects.[1] However, the clinical success of these modalities are usually limited by availability, donor site morbidity, and potential disease transmission.[2] To overcome these limitations, there are growing interests and needs to develop synthetic bone substitutes that can be used as alternatives to these conventional modalities for skeletal repair. Thus, considerable recent effort has been devoted to the development of novel bioactive materials with intrinsic biocompatible, biodegradable, and osteogenic properties.

Over the past decades, a variety of bioactive inorganic materials have been developed for bone tissue regeneration purposes, such as bioceramics, bioactive glasses, hydroxyapatite (HA), β-tricalcium phosphate (TCP) and so on.[3−5] Recently, silica-based materials in different forms, such as silica thin films, silica nanofibers, silica xerogel, and silica nanoparticles, were also proposed as potential bone substitutes.[6−8] Among them, mesoporous silica nanoparticles (MSNs) have been extensively explored for biomedical applications due to their superior features such as high specific surface areas, large pore volumes, controllable particle size, accessible surface functionalization and favorable biocompatibility.[9−12] These properties make them very interesting as excellent candidates for drug delivery, cell targeting, and gene therapy.[13] It is well-known that natural bone is comprised of collagen and nanohydroxyapatite.[14,15] The size of MSNs can be tuned over a broad range, which is considered to easily match the size range of the integral parts (such as hydroxyapatite crystals) of natural bone, making them promising candidates for bone tissue repair.[16]

Received: March 26, 2015
Accepted: July 2, 2015
Published: July 2, 2015

DOI: 10.1021/acsami.5b02636
ACS Appl. Mater. Interfaces 2015, 7, 15777−15789

Bone formation is a complex process that is regulated by the systemic hormones, local production of cytokines, and various growth factors.[6,14] As a consequence, the surface functionalization with growth factors or direct incorporation of growth factors into the materials has been demonstrated to be effective in improving the cell adhesion and osteoblast differentiation on materials.[17−19] The osteogenic growth factors typically include various bone morphogenetic proteins (BMPs, such as BMP-2, BMP-6, BMP-7 and BMP-9), transforming growth factors β (TGF-β), platelet-derived growth factor (PDGF), insulin-like growth factor (IGF) and so on.[6,14] BMPs, the most potent osteoinductive growth factors, belong to the TGF-β superfamily.[20] In particular, recombinant human bone morphogenetic protein-2 (BMP-2), have demonstrated an impressive ability to induce new bone formation in vivo.[21] However, BMP-2 protein is degraded rapidly in the body by proteinases, and thus, high doses of BMP-2 possibly cause adverse effects, such as ectopic bone formation, immunological reaction, and even tumorigenesis.[22] As a means to reduce protein diffusion from the integration site and increase the efficacy, immobilization of BMP-2 onto nanoparticles has attracted great interest.[23] For example, BMP-2 entrapped in dextran-derived microspheres induced higher expression of alkaline phosphatase in human periodontal ligament cells, and could achieve a longer action time than the aqueous solution with equivalent BMP-2 concentration.[24] BMP-2 incorporated hydroxyapatite nanoparticles have been developed as controlled-release carriers, showing a sustained release profile of BMP-2.[25] Neumann et al. showed that BMP-2 loaded onto nanoporous silica nanoparticles possessed a higher osteoinductive effect in human mesenchymal stem cells compared to BMP-free nanoparticles.[26] Additionally, BMP-2 protein was also immobilized onto chitosan-functionalized MSNs to induce osteoblast differentiation,[27] The result indicated that more than 80% of BMP-2 was released within 24 h and thus yielded a much higher localized concentration of protein on the cell surface and possible side effects. This limitation may be overcome by using the osteogenic BMP peptide to reduce the undesired side effect of BMP protein.[28,29] Saito et al. reported that the synthetic peptide KIPKASSVPTELSAISTLYL corresponding to residues 73−92 of the knuckle epitope of BMP-2 significantly elevate alkaline phosphatase activity than other residue sequences in C3H10T1/2 cells.[30] They further demonstrated that the 73−92 peptide-conjugated alginate gel remained active at the implanted site and activated osteoblasts to promote ectopic calcification.[31] Further studies demonstrated that incorporating the BMP-2 peptide in biomaterials can induce in vitro osteogenic differentiation and in vivo bone regeneration.[5,32−34]

The combined therapy with growth factors and bone therapeutic drugs has already been proven effective in bone tissue engineering. Dexamethasone (DEX), a synthetic glucocorticoid, is the earliest and more readily osteogenic inducers for bone marrow stromal cells.[35] Combination treatment with DEX and BMP-2 protein was also demonstrated to be an effective stimulator to enhance the BMP-2-induced osteoblast differentiation.[18,27] Thus, we hypothesize that the simultaneous incorporation of bioactive DEX and BMP-2 peptide into the MSNs may exert synergistic effect on osteoblast differentiation of bone mesenchymal stem cells (BMSCs).

In this study, BMP-2 derived peptide-functionalized and DEX-loaded MSNs were developed to evaluate their effect on the osteogenic differentiation of BMSCs. The BMP-2 peptide functionalized MSNs were first synthesized by covalently grafting the peptide with aminated MSNs, and DEX was then entrapped into the mesoporous channels of MSNs to construct osteogenic factor delivery vehicles. The effect of BMP-2 peptide grafting on the cellular uptake of MSNs was extensively explored, and the in vitro and in vivo osteogenic effect of the resulting osteogenic factor delivery vehicles were also investigated.

2. MATERIALS AND METHODS

2.1. Materials. Tetraethyl orthosilicate (TEOS), cetyltrimethylammonium bromide (CTAB), 3-aminopropyltriethoxysilane (APTES), fluorescein isothiocyanate (FITC), 1-ethyl-3(3-(dimethylamino)propyl) carbodiimide (EDC), *N*-hydroxysuccinimide (NHS), dexamethasone (DEX), and Alizarin Red S were purchased from Sigma-Aldrich Trading Co., Ltd. (Shanghai, China). The fluorescein isothiocyanate labeled BMP-2 peptide (FITC-KIPKASSVPTELSAISTLYL sequence) was synthesized from Chinapeptides Co., Ltd. (Shanghai, China). Fetal bovine serum (FBS), penicillin-streptomycin, trypsin and DMEM/F12 were obtained from Gibco Life Technologies Co. (Grand Island, NY). Deionized water was used in all experiments. All chemicals were used without further purification.

2.2. Synthesis of MSNs and FITC-Labeled MSNs. MCM-41 type MSNs were prepared by modifications of previously reported methods.[36] Typically, 1.0 g of CTAB and 0.28 g of NaOH were dissolved in 480 mL of deionized water. The mixture solution was heated to 80 °C and stirred vigorously. Then, 5.0 mL of TEOS was added dropwise to the surfactant solution under vigorous stirring at 80 °C for 2 h. The products were collected by centrifugation and washed several times with water and ethanol. Subsequently, the surfactant templates were removed by extraction in acidic ethanol (5 mL of HCl in 500 mL of ethanol) for 24 h. The surfactant-free MSNs were collected by centrifugation and dried under vacuum.

To obtain FITC-labeled MSNs, FITC-conjugated APTES (FITC-APTES) was first synthesized by reacting of FITC (4 mg) with APTES (44 μL) in 1.0 mL of ethanol under dark conditions for 24 h. After that, 0.5 mL of FITC-APTES solution was added before TEOS in the synthetic process of MSNs. Finally, the surfactant-free FITC-labeled MSNs were dried under vacuum for further use.

2.3. Preparation of Aminated MSNs (MSNs-NH_2). The surface of MSNs was functionalized with amine groups by treatment with APTES. One gram (1 g) of MSNs was first dispersed in 200 mL of anhydrous ethanol, and then the solution was heated to 80 °C and stirred for 2 h, followed by the addition of 2 mL APTES. After refluxed for 24 h, the solution was centrifuged and washed with water for several times. Finally, the MSNs-NH_2 was redispersed in water for further use.

2.4. BMP-2 Peptide Functionalized MSNs (MSNs-pep). For the synthesis of BMP-2 peptide functionalized MSNs, the peptide was covalently grafted onto the surface of MSNs-NH_2 through the reaction of −COOH and −NH_2 group by using cross-linking reagents as described previously.[37] First, 200 μg of peptide was added into sterile PBS solution (pH 7.4), followed by the addition of 0.2 mmol of EDC and 0.5 mmol of NHS. After the mixture was stirred for 30 min at room temperature, 20 mg of sterilized MSNs-NH_2 which dispersed in 20 mL of PBS solution was added to the solution and stirred for another 24 h. Then, the solution was centrifuged and washed with deionized water for several times to remove the excess EDC, NHS, and peptides. The as-prepared MSNs-pep was dispersed in sterile water and stored at 4 °C. The excess FITC labeled BMP-2 peptide were collected to determine the mass of the graft by UV−vis spectra at 495 nm using a calibration curve constructed from known concentrations of BMP-2 peptide, approximately 79.8% of peptide were grafted on MSNs.

2.5. Characterization. Morphology and structure of nanoparticles were observed with a JEM-2100F (Jeol Ltd., Japan) transmission electron microscope (TEM) operating at 200 kV. Attenuated total reflectance-Fourier transform infrared (ATR-FTIR) spectroscopy was

DOI: 10.1021/acsami.5b02636
ACS Appl. Mater. Interfaces 2015, 7, 15777−15789

recorded on Nicolet 6700 (Thermo, Waltham, MA). Small-angle X-ray diffraction (SAXRD) pattern was obtained using a D/MAX-2550PC (Rigaku Inc., Japan) diffractometer with the CuKα radiation at 45 kV and 40 mA. The size distribution of the nanoparticles was measured by dynamic light scattering (DLS) using a BI-200SM multiangle dynamic/static laser scattering instrument (Brookhaven, Holtsville, NY). The zeta potential measurements were performed on a Zetasizer Nano ZS instrument (Malvern, UK). UV−vis spectra were recorded on a Jasco V530 UV−vis spectrophotometer (Jasco, Japan).

2.6. DEX Loading and in Vitro Release. For DEX loading, 0.2 g of MSNs or MSNs-pep was added to 20 mL of DEX solution (0.1 mg/mL, dissolved in PBS solution) and the mixture was stirred at room temperature for 24 h. Then, the soaked nanoparticles were vacuumed at room temperature for another 2 h. The DEX-loaded nanoparticles (DEX@MSNs or DEX@MSNs-pep) were collected by centrifugation and washed three times with PBS. The supernatant and the washing solutions were collected together to determine the DEX loading using UV−vis spectra at 242 nm. The loading amount of DEX was determined to be 1.5 and 1.7 μg/mg for DEX@MSNs and DEX@MSNs-pep, respectively.

In vitro release of DEX from DEX@MSNs-pep was carried out in PBS solution (pH 7.4). The DEX loaded nanoparticles (20 mg) were suspended directly in 1 mL of PBS in the dialysis bag (cutoff molecular weight 3500 Da) and the bag was placed in a centrifuge tube containing 4 mL PBS, and then shaken at a speed of 100 rpm at 37 °C. The amount of DEX released in the medium was monitored via UV−vis spectra at 242 nm.

2.7. BMSCs Isolation and Culture. Four-week-old female Sprague−Dawley (SD) rats were obtained from Shanghai Laboratory Animal Center (Shanghai, China). Rat BMSCs were isolated from the femurs and tibias of SD rats as described previously,[38] which was performed in compliance with the protocols approved by the Institutional Animal Care and Use Committees (IACUC) guidelines. BMSCs were cultured in DMEM/F12 containing 10% FBS and 1% penicillin/streptomycin at 37 °C in 5% CO_2. The fourth to sixth passage cells were used for the following experiments.

To investigate the bioactivity of different samples, BMSCs were seeded at a density of 1×10^4 cells/cm^2 and incubated in 5% CO_2 at 37 °C. After the cells reached 80% confluence, the medium were replaced with different sample suspensions. BMSCs cultured in normal medium (Normal, DMEM/F12 + 10% FBS + 1% penicillin/streptomycin) and osteoconductive medium (normal medium supplemented with 10 mM β-glycerol phosphate and 50 μg/mL of L-ascorbic acid) were used as controls. The experimental samples (BMSCs and nanoparticles) were maintained in osteoconductive medium. The cell culture medium was replaced every 3 days.

2.8. Cell Viability Assay. The viability of BMSCs was assessed using Cell Counting Kit-8 (CCK-8) assays. Briefly, BMSCs were seeded in 96-well plates with 100 μL of medium at a density of 5×10^3 cells per well, and cultured in 5% CO_2 at 37 °C. After seeding for 24 h, cells were washed with PBS, and exposed to various concentrations of samples (6.25, 12.5, 25, 50, and 100 μg/mL). After incubation for 24 and 48 h, 10 μL of CCK-8 solution was added into each well, and the cells were incubated for another 2 h at 37 °C. The absorbance was measured at 450 nm with a plate reader (Multiskan MK3, Thermo). A culture medium without nanoparticles was used as the control. The cytotoxicity was expressed as the percentage of the cell viability as compared with the control.

2.9. Analysis of Intracellular Uptake. For confocal laser scanning microscope (CLSM, Carl Zeiss LSM 700) observations, BMSCs (1×10^5 cells per dish) were seeded in 20 mm glass bottom culture dishes and incubated for 24 h. After that, the medium was removed and the cells were incubated with FITC-conjugated samples (50 μg/mL) at 37 °C for specific time points. After being washed several times with PBS, cells were fixed with 4% paraformaldehyde for 10 min at room temperature. The cells were washed three times with PBS and incubated with 0.1% Triton X-100 and then 1% bovine serum albumin (BSA) in PBS for 5 and 30 min, respectively. Alexa Fluor 568 phalloidin was used for staining the actin filaments for 20 min at room temperature. The nucleus was stained with DAPI (Bestbio, Shanghai) for 5 min. Then, the samples were observed by CLSM.

For the quantification of intracellular uptake of nanoparticles, flow cytometry (FCM) was used to detect the FITC signal in BMSCs. BMSCs were seeded at 1×10^5 cells on each six-well culture plate and cultured for 24 h. Then the cells were treated with samples (50 μg/mL). After 24 or 48 h of incubation, the medium was totally taken out and cells were washed with PBS and trypsinized. The cells were collected by centrifugation at 2000 rpm, washed with PBS three times, and resuspended in 1 mL of PBS. Then cell suspensions were filtered through 400-mesh sieves and finally subjected to a FACSCalibur flow cytometry (BD Biosciences). To investigate the ligand−receptor interaction of BMP-2 peptide and its receptors, we introduced noggin (Genscript, Nanjing). The cells were treated with MSNs-pep containing noggin (200 ng/mL) for 24 h and followed by the same procedure as above.

In addition, the mass of nanoparticles in BMSCs was measured by detecting the silicon concentration with inductively coupled plasma optical emission spectroscopy (ICP-OES) (Prodigy, Leeman Laboratories). BMSCs (2×10^6) were seeded in a 10 cm Petri dish and incubated for 24 h. Then the cells were treated with samples (100 μg/mL) for 24 h. After removal of the supernatant and washing several times with PBS, the cells were trypsinized, and then were centrifuged and washed three times. After the cells were dried overnight, the cells were treated with 0.1 mL of 40 wt % HF with ultrasound, followed by the addition of 9.9 mL of 2 wt % HNO_3 aqueous solution. Finally, the clear solutions were used to measure the silicon concentration by ICP-OES.

To study the endocytosis of nanoparticles, we used a protocol described previously.[12] The cells were finally observed with a JEM-2100 TEM.

2.10. Alkaline Phosphate (ALP) Activity. ALP activity of BMSCs was evaluated by an assay kit (Beyotime Institute of Biotechnology, China), which quantified the conversion of p-nitrophenol phosphate (pNPP) to yellow p-nitrophenol (pNP) by ALP enzyme. Briefly, after being exposed to samples at predetermined time points, the cells were lysed with cell lysis buffer. Next, 50 μL cell lysates were added into a 96-well plate containing 50 μL substrate solutions and incubated at 37 °C for 30 min. Then, the stop solution was added to terminate the reaction. The absorbance was read at 405 nm with a plate reader. The ALP concentrations were determined by a standard curves. For normalization, the total protein concentration was measured by a protein assay kit (Beyotime Institute of Biotechnology, China).

2.11. Alizarin Red S (ARS) Staining. At the predetermined time points after the addition of nanoparticles, BMSCs were fixed with 10% formalin for 20 min and then washed three times with PBS. The fixed cell were further washed with distillated water to remove any salt residues before covered in 2% (wt/v) ARS with a pH adjusted to 4.1−4.3. After an incubation of 10 min at room temperature, samples were washed until the excess of ARS was removed. The ARS staining was imaged using a camera (Canon EOS 550D). To quantify coloration of ARS, we added 10% acetic acid to the samples. After an overnight incubation, the samples were transferred to tubes and centrifuged for 15 min at 13 000 rpm. Then, the supernatant was extracted to other tubes and neutralized with 10% ammonium hydroxide, and 100 μL of each sample was added to 96-well plates and read at 405 nm with a plate reader.

2.12. Immunocytochemistry. At the predetermined time points after the addition of nanoparticles, BMSCs were fixed with 10% formalin for 20 min. Cells were then permeabilized with 0.1% Triton X-100 solution for 5 min and nonspecific binding blocked with 10% normal donkey serum for 30 min. Cells were incubated overnight at 4 °C with the primary antibodies: mouse antihuman/rat osteocalcin monoclonal antibody (1:50 dilution, R&D, Minneapolis, MN) and RUNX2 (D1L7F) rabbit mAb (Cell Signaling Technology, Beverly, MA). After that, cells were washed three times with PBS and treated for 1 h with the appropriate secondary antibody: donkey antimouse IgG NL557 (1:200 dilution, R&D, Minneapolis, MN) and donkey antirabbit IgG H&L (Alexa Fluor 405; 1:200 dilution, Abcam,

DOI: 10.1021/acsami.5b02636
ACS Appl. Mater. Interfaces 2015, 7, 15777−15789

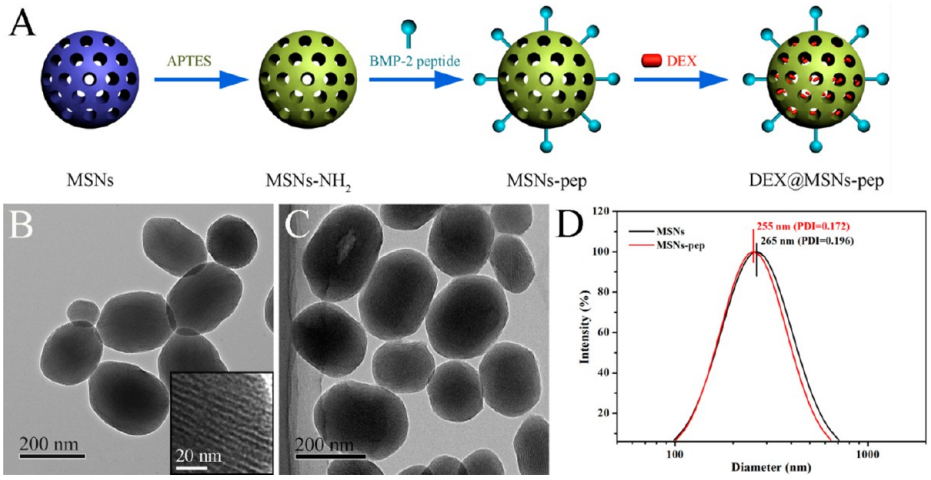

Figure 1. (A) Schematic illustration for the preparation of DEX@MSNs-pep; TEM images of (B) MSNs (inset is the enlarged image) and (C) MSNs-pep; and (D) size distribution of MSNs and MSNs-pep.

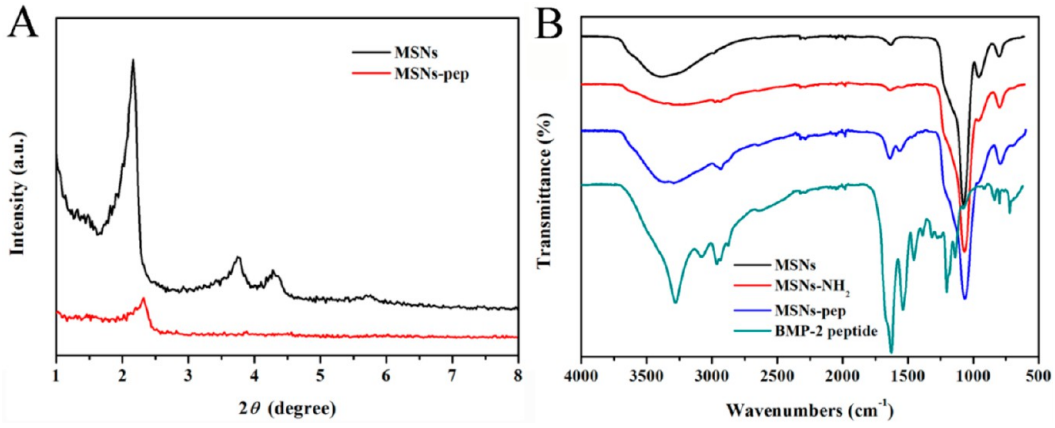

Figure 2. (A) Small-angle XRD patterns of MSNs and MSNs-pep; (B) ATR-FTIR spectra of MSNs, MSNs-NH_2, MSNs-pep, and BMP-2 peptide.

England). Negative control samples were not subjected to primary antibody incubation. After being washed three times with PBS, the nucleus was respectively stained with 4′,6-diamidino-2-phenylindole (DAPI) and propidium iodide (PI).

2.13. Ectopic Bone Formation in Vivo. The animal experiments were performed on 4-week-old male SD rats (Silaike Inc. Shanghai, China) and conducted as reported previously.[27] The implanted materials were divided into three groups: (1) Gelfoam loaded with MSNs; (2) Gelfoam loaded with MSNs-pep; (3) Gelfoam loaded with DEX@MSNs-pep. The content of BMP-2 peptide and DEX within the implants was 100 and 20 μg, respectively. These materials were prepared by adsorbing the particles solution into gelfoam and then dried for further use. The rats were divided into three groups (each group: n = 6), anesthetized with an intraperitoneal injection of pentobarbital (0.06 g/kg) and implanted with the prepared materials into right thigh muscle pouches. Three weeks postoperation, the rats were examined by a dual-source computed tomography (CT) system (Somatom Definition Flash, Simens, Germany) to evaluate the bone formation. Imaging parameters were as the follows: thickness, 0.6 mm; kVp, 80; effective mAs, 110; FOV, 20 cm.

After implantation for 3 weeks, the implants were harvested together with the surrounding muscles. Each specimen was fixed with 10% neutral formalin. Then the specimen was sectioned at 5 μm thick and stained with hematoxylin/eosin (HE). All the samples were observed using a microscope.

2.14. Statistical Analysis. All experiments were conducted at least three times, and data are presented as mean ± standard deviation (SD). Statistical analysis was carried out using the one-way analysis of variance (ANOVA) followed by post hoc Tukey's method to test all pairwise mean comparisons. The statistical significance for all tests were considered at $^*P < 0.05$ and $^{**}P < 0.01$.

3. RESULTS AND DISCUSSION

3.1. Preparation and Characterization of MSNs-pep. BMPs are the most widely used cytokines promoting osteogenic differentiation of mesenchymal stem cells. Many short peptide sequences derived from BMPs, such as BMP-2 peptide, BMP-7 peptide, or BMP-9 peptide,[5,39] were demonstrated to have bioactivity similar to the full length BMPs. Thus, we are interested in the influence of BMP-2 peptide conjugated MSNs on the osteogenic differentiation activity of BMSCs. In this study, a facile route was used to prepare MSNs-pep as schematically described in Figure 1A. Briefly, MSNs were synthesized by a surfactant-based method, followed by introducing the APTES to obtain aminated MSNs. For the preparation of MSNs-pep, the BMP-2 derived peptide was covalently grafted onto the aminated MSNs through the reaction of carboxy and amino group by using cross-linking reagents. Subsequently, MSNs-pep was immersed into DEX solution with stirring to obtain DEX-loaded sample.

TEM image in Figure 1B clearly displays the morphology and structure of the resulting MSNs. MSNs exhibited a round or elliptic morphology with highly ordered mesoporous channels (Figure 1B and inset). After grafting with peptide, a very thin polymeric shell was formed on the exterior surface of

DOI: 10.1021/acsami.5b02636
ACS Appl. Mater. Interfaces 2015, 7, 15777−15789

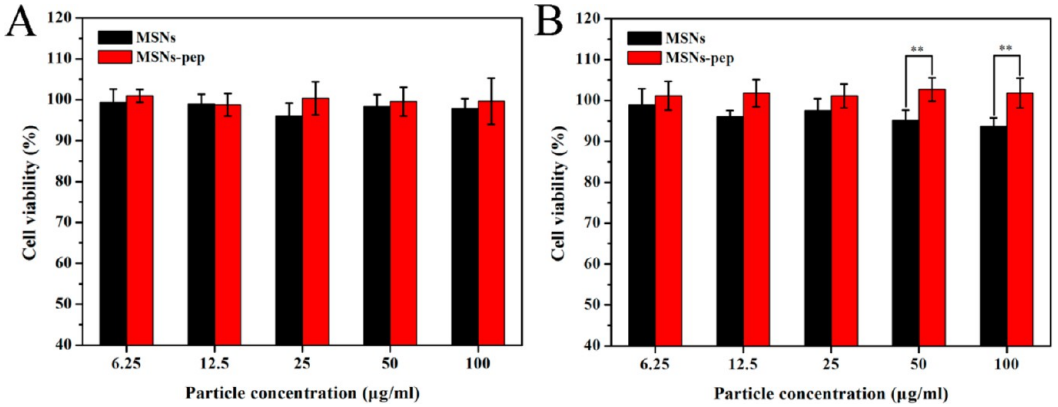

Figure 3. Cell viability of BMSCs cultured with different concentrations of MSNs and MSNs-pep for (A) 24 h and (B) 48 h. Cell viability was expressed as the percentage of the untreated control group.

MSNs (Figure 1C). The hydrodynamic diameter and size distribution of MSNs and MSNs-pep were measured by DLS. As shown in Figure 1D, the mean hydrodynamic diameter of MSNs was 265 nm with the polydispersity index (PDI) of 0.196. It was note that a smaller hydrodynamic diameter of 255 nm and a narrower PDI of 0.172 of MSNs-pep were observed, which indicates that MSNs-pep have better dispersibility because of peptide grafting. To further verify this point, MSNs and MSNs-pep were respectively dispersed in different solutions, including water, PBS solution and medium (serum-containing cell culture medium). We observed that MSNs could be readily dispersed in water, while sediment was appeared when dispersed in PBS or medium (Figure S2, SI). Obviously, whatever water, PBS or medium, MSNs-pep all exhibit a well-dispersed state, indicating that the dispersibility and stability of MSNs-pep were significantly improved in PBS or medium compared with that of MSNs.

As shown in Figure 2A, the SAXRD pattern of MSNs showed an intense peak and three weaker peaks, assigned as (100), (110), (200), and (210) planes, respectively, which is the characteristic diffraction pattern of MCM-41 type MSNs, indicating that the synthesized MSNs have hexagonal type of mesoporous structure.[9] Compared with bare nanoparticles, the intensity of the diffraction peaks decreased sharply after peptide grafting (Figure 2A). Nevertheless, MSNs-pep showed the characteristic diffraction peaks at (100) plane, which implies that peptide functionalized MSNs still possess an ordered 2D hexagonal structures. This change of SAXRD result confirms the successful surface functionalization.[40] Figure 2B shows the FTIR spectra of the samples before and after peptide grafting. Compared with bare MSNs, the peak at 959 cm^{-1} ascribing to the stretching vibration of Si−OH is evidently decreased in intensity on the spectrum of aminated MSNs, while a new peak at 1548 cm^{-1} corresponding to N−H asymmetric bending appeared due to the successful modification of MSNs with amino groups.[41] After grafting with peptide, the new peak appeared at 2935 cm^{-1} and the enhanced peaks at 1638 and 1562 cm^{-1}, which correspond to the C−H stretching vibration, C═O stretching vibration of amide I, and N−H bending vibration of amide II,[42] respectively, indicating the successful grafting of peptide. In addition, UV−vis spectra measurement was utilized to confirm the successful grafting of peptide on the outer surface of MSNs rather than the adsorption. As shown in Figure S1 (SI), the prepared MSNs-pep suspension dispersed in deionized water showed yellow solution and displayed the characteristic absorption band of FITC. After centrifugation, as MSNs-pep nanoparticles were precipitated in the bottom of the centrifuge tube, the supernatant become transparent and the characteristic peak of FITC was disappeared. This result was consistent with previous report and confirmed the successful incorporation of BMP-2 peptide on the aminated MSNs by conjugation reaction.[37]

3.2. Cytotoxicity Assay. It is essential to investigate the cytotoxicity of the prepared nanoparticles prior to the evaluation of osteogenic differentiation activity. Therefore, in vitro cytotoxicity of the peptide functionalized MSNs against BMSCs was assessed using CCK-8 assay and the bare MSNs was used as a control. As shown in Figure 3, the effects of bare MSNs and MSNs-pep on the viability of BMSCs were studied at various doses (6.25, 12.5, 25, 50, and 100 μg/mL). It could be observed that both MSNs and MSNs-pep showed no obvious cytotoxicity on the BMSCs at 6.25−100 μg/mL after incubation for 24 and 48 h (Figure 3A,B). Furthermore, MSNs-pep showed significantly higher cell viability than MSNs at the concentrations of 50 and 100 μg/mL after incubation for 48 h ($P < 0.01$). For 48 h incubation, as the particle concentration of MSNs was as high as 100 μg/mL, the cell viability was about 93.7%. These results demonstrated that MSNs-pep possess better biocompatibility and will not cause obvious cytotoxic effect once the BMP-2 peptide is shed in vivo. Therefore, MSNs-pep is highly cytocompatible and can be kindly used in the following experiments.

3.3. Intracellular Uptake of Nanoparticles. BMSCs were incubated with MSNs and MSNs-pep at the concentration of 50 μg/mL. The uptake of these nanoparticles by BMSCs was first analyzed by CLSM (Figure 4). After 24 h exposure, BMSCs were generally well-spread, and there were no any adverse effects on the cell cytoskeleton compared to the untreated control cells. The green fluorescence of the labeled FITC enables the visualization of the cellular uptake of nanoparticles. The results from the cellular uptake are illustrated in Figure 4. It can be clearly seen that the cellular uptake was increased from 24 to 48 h, suggesting a time-dependent pattern. Importantly, there were more green spots distributed in the cytoplasm of BMSCs which were incubated with MSNs-pep nanoparticles than those incubated with MSNs, which indicated that BMSCs can take up more BMP-2 peptide grafted MSNs nanoparticles than bare MSNs. This result indicates that BMP-2 peptide grafting may enhance the delivery of MSNs-pep into the cytoplasm of BMSCs. To verify this

DOI: 10.1021/acsami.5b02636
ACS Appl. Mater. Interfaces 2015, 7, 15777−15789

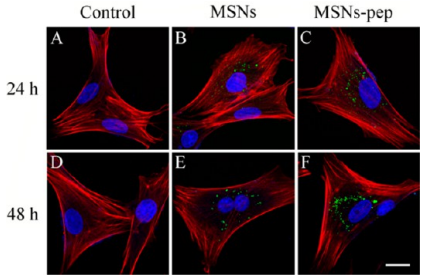

Figure 4. Confocal microscopy images of BMSCs incubated with different samples for (A–C) 24 and (D–F) 48 h. Cells cytoskeleton was stained for actin filament using Alexa Fluor 568 phalloidin (red). The cells nuclei were stained using DAPI (blue). Green fluorescence indicates the nanoparticles. (A and D) Control, without nanoparticles treating; (B and E) MSNs; and (C and F) MSNs-pep. Images were obtained with a 63× oil-immersion objective (scale bar = 20 μm).

phenomenon, we used flow cytometry to quantify the cellular uptake of nanoparticles via the green fluorescence signal of FITC after the cells were treated with nanoparticles for 24 and 48 h. As shown in Figure 5A,B, the mean fluorescence intensity increased with increasing the incubation time for both nanoparticles. However, at the same culture time and the same nanoparticles concentration, MSNs-pep exhibited a significant increase in fluorescence intensity when compared to the bare MSNs ($P < 0.01$) (Figure 5B). In addition, the percent population of cells uptaken with FITC labeled nanoparticles was also used to evaluate the cellular uptake of samples. From Figure 5C, we can see that the overall uptake for MSNs-pep was significantly higher than that for MSNs ($P < 0.01$), suggesting that BMP-2 peptide grafting greatly enhanced the cellular uptake efficiency.

To further clarify the difference of intracellular uptake between MSNs-pep and MSNs, the uptake of nanoparticles distributed in the BMSCs can be evidenced by TEM images. As shown in Figure 6A–D, large numbers of nanoparticles (white arrows) were found in the cytoplasm while no nanoparticles were found in the nucleus, and they still maintained the elliptic morphology. In addition, part of the nanoparticles could be found in the vesicular compartments near the cell membrane (Figure 6D). It is reported that the silica-based nanoparticles could be processed in endosomes and lysosomes after the uptake by cells via endocytosis, and were eventually released into the cytoplasm.[10,43] Noticeably, the mesoporous structure in the uptaken MSNs can be clearly seen (Figure 6B) but not in MSNs-pep (Figure 6D), which was consistent with the previous TEM observation. Moreover, as expected, the TEM images

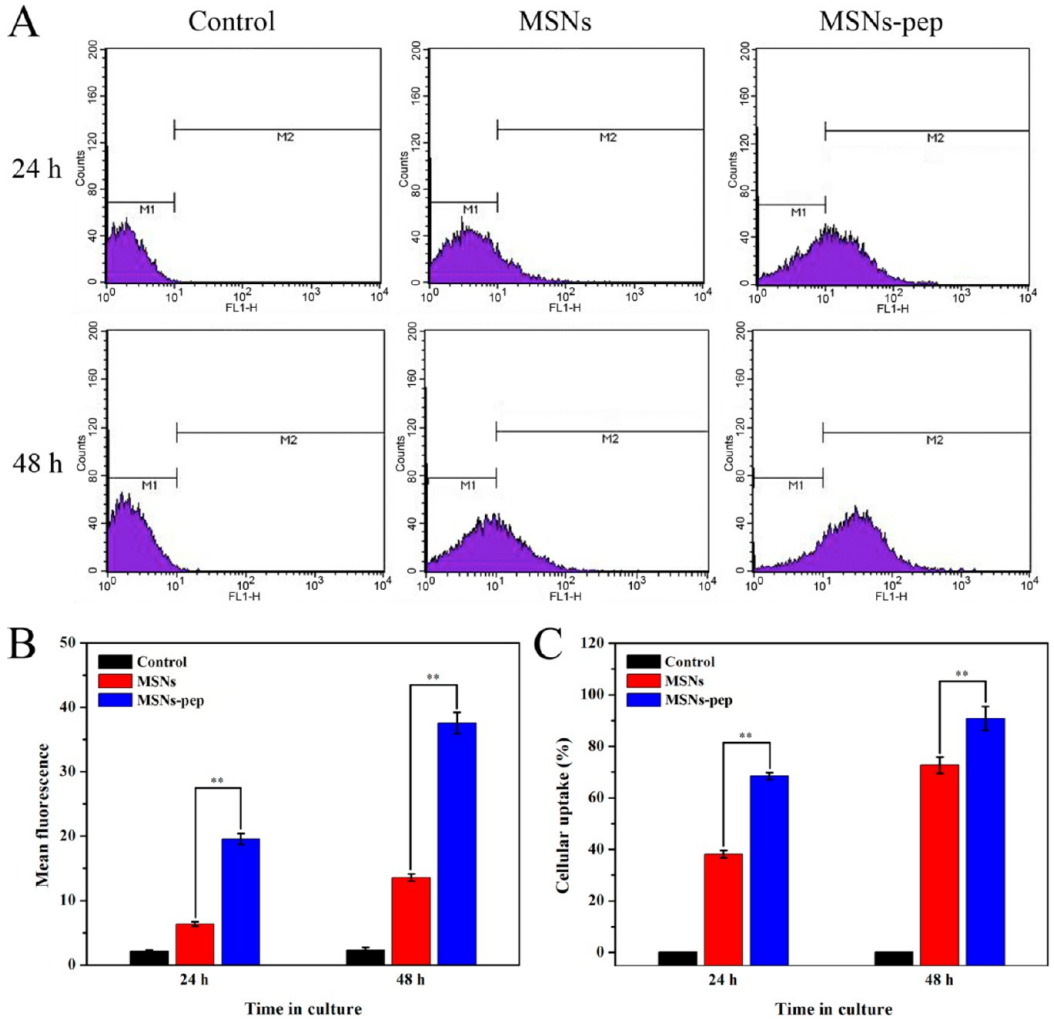

Figure 5. In vitro cellular uptake of MSNs and MSNs-pep against BMSCs for 24 and 48 h. (A) Flow cytometry assays of cellular uptake, (B) mean fluorescence intensity, and (C) cellular uptake percentage of MSNs and MSNs-pep.

DOI: 10.1021/acsami.5b02636
ACS Appl. Mater. Interfaces 2015, 7, 15777–15789

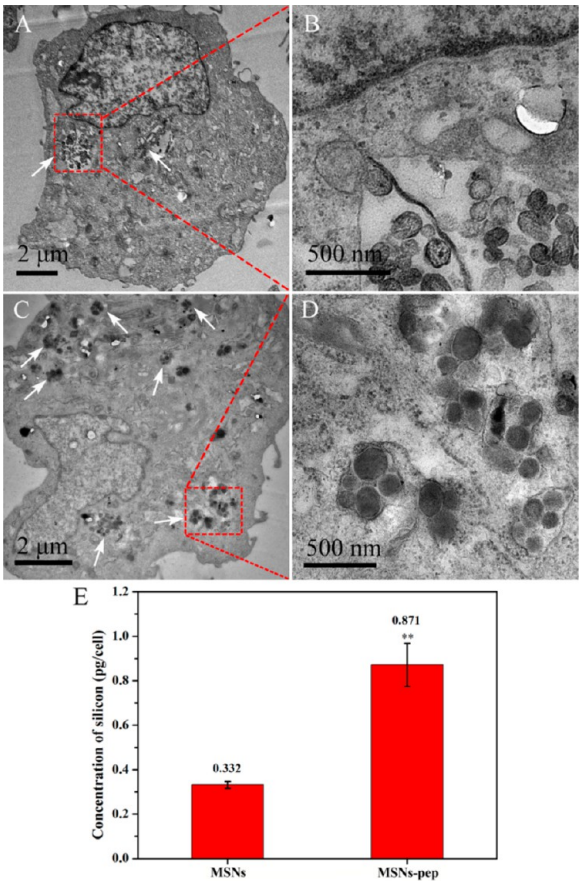

Figure 6. Effect of functionalization on MSN uptake. TEM investigation of (A and B) MSNs and (C and D) MSNs-pep uptaken in BMSCs, nanoparticles indicated by white arrows; (E) mass of silicon internalized in BMSCs measured by ICP-OES technique.

show that more MSNs-pep nanoparticles are internalized in BMSCs compared to the bare MSNs. In addition, as shown in Figure S3 (SI), the side-view from z-stack images obtained by confocal microscopy also reveal the difference of intracellular uptake between MSNs-pep and MSNs. Compared with the MSNs group, we found that more MSNs-pep nanoparticles were resided in the cytoplasm of BMSCs. To quantitatively determine the cellular uptake of these nanoparticles, ICP-OES was used to measure the mass of nanoparticles in BMSCs. Figure 6E shows the mass of silicon internalized per cell obtained from ICP-OES measurements, which was 0.33 and 0.87 pg/cell for MSNs and MSNs-pep nanoparticles, respectively. Obviously, the uptake amount of MSNs-pep was nearly 3 times than that of MSNs. The above results also confirmed that BMP-2 peptide grafting could enhance the cellular uptake of MSNs-pep by BMSCs.

As reported previously, noggin is the specific inhibitor of BMP, which prevents BMP binding to the cell surface receptors by binding to BMP with high affinity.[44] To investigate whether the enhanced cellular uptake of MSNs-pep was depended on the ligand−receptor interaction of BMP-2 peptide and its receptors, we performed further studies by introducing noggin to block the ligand−receptor interaction. As shown in Figure S4 (SI), in the case of MSNs-pep with and without the presence of noggin, they did not show a statistically significant difference on the fluorescence intensity. Nevertheless, because of the presence of noggin, the cellular uptake of MSNs-pep was lower than that of alone MSNs-pep. In theory, however, the cellular uptake of MSNs-pep may be dramatically decreased because of the existence of inhibitor, but the experimental result appears to be somewhat different. We deduced that the ligand−receptor interaction between peptide and receptors may be an important factor influencing cellular uptake of MSNs-pep. In addition, the positively charged character of the MSNs-pep (Figure S5, SI), which may facilitate the interaction between cells and nanoparticles, and therefore reduced the inhibiting effect of noggin.

3.4. ALP Activity Quantification. In this study, BMP-2 peptide was grafted onto the surface of MSNs to enhance the osteogenic differentiation activity of BMSCs. DEX is a synthetic glucocorticoid which has also served as a bioactive agent to promote osteogenic differentiation of mesenchymal stem cells.[45] Thus, the release of DEX from DEX@MSNs-pep may result in higher osteogenic differentiation activity than single use of MSNs-pep. We therefore compared the osteoblastic differentiation activity of BMSCs which were incubated with different nanoparticles (loaded or unloaded with DEX). Normally, ALP activity was measured as a marker of osteogenic differentiation, and the upregulation of ALP activity is a key event occurring during the early time points of osteogenesis.[46] Figure 7 shows the in vitro ALP activity of BMSCs treated with different samples for different culture time. It can be seen that ALP activity increased with increasing culture time for all the test groups. The addition of MSNs-pep, DEX@MSNs and DEX@MSNs-pep nanoparticles (50 μg/mL, containing about 400 ng/mL of BMP-2 peptide) significantly enhanced the ALP activity compared with other groups at day 21 ($P < 0.01$), which demonstrated that the introduction of these nanoparticles within the extra- and intracellular environment can trigger the upregulation of ALP. As expected, BMSCs treated with DEX@MSNs-pep showed the higher ALP activity than the cells treated with MSNs-pep, due to the presence of DEX, known for triggering the osteogenic differentiation. Additionally, the ALP activity of DEX@MSNs-pep group was obviously higher than that of the DEX@MSNs. Moreover, at day 14, it was noted that the ALP activity of cells treated with DEX@MSNs-pep was higher than other samples. We also investigated the effect of nanoparticles concentration on ALP activity. As shown in Figure 7B, higher ALP activity in MSNs-pep group was obtained within the tested concentrations compared to the control (without nanoaprticles in osteoconductive medium) at day 21 ($P < 0.01$), and the ALP activity increased with the increase of particle concentration. A similar trend in ALP activity was observed in DEX@MSNs-pep group and almost 2-fold increase was observed at concentration of 50 μg/mL compared to the control at day 21. However, at the particle concentration of 100 μg/mL, a decrease in ALP activity was observed, but it still showed higher ALP activity than the control. To further investigate this result, the in vitro release of DEX from DEX@MSNs-pep was detected. As shown in Figure S6 (SI), the result showed that DEX was released in a sustaining manner and the amount of released DEX reached to 61.3% at day 27, indicating that the released DEX could effectively maintain the proper concentration to stimulate the osteogenic differentiation of BMSCs. At day 3, the amount of released DEX was 23.6%, making the DEX concentration over 10^{-7} M. Given that the maximally stimulatory effects of DEX on osteoblast differentiation are 10^{-8} to 10^{-7} M, on the one hand, the decrease in ALP activity may be that high concentrations of DEX down-regulate its receptors, then

DOI: 10.1021/acsami.5b02636
ACS Appl. Mater. Interfaces 2015, 7, 15777−15789

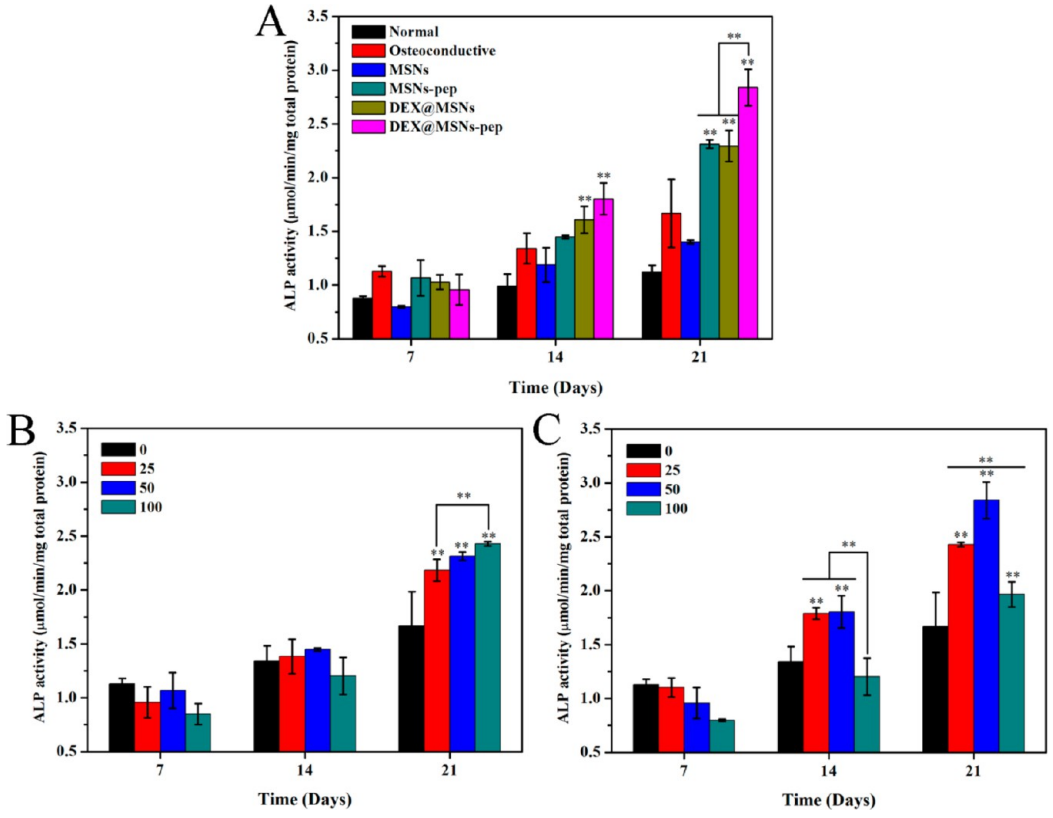

Figure 7. (A) In vitro alkaline phosphatase (ALP) activity of BMSCs after treated with various samples for different culture period, (B) different concentrations of MSNs-pep and (C) different concentrations of DEX@MSNs-pep. Data were analyzed using one-way ANOVA against the osteoconductive group.

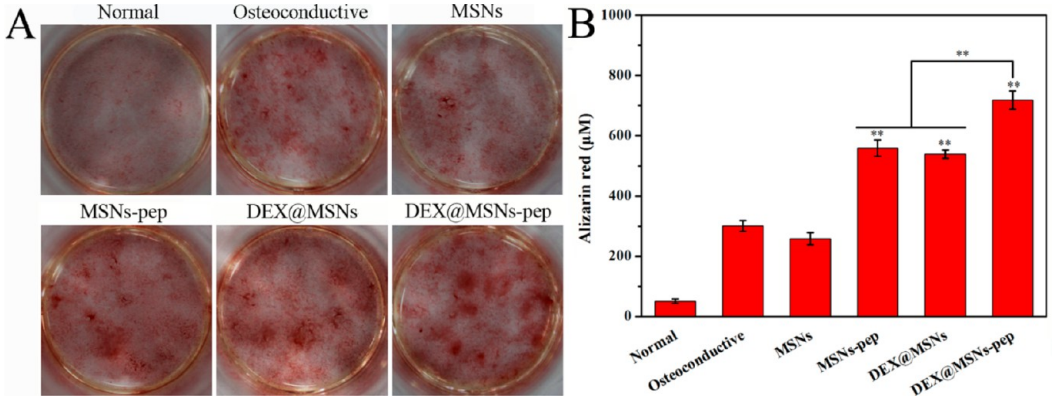

Figure 8. Evaluations of the mineralized extracellular matrix produced by BMSCs under osteogenic induction. The mineralized matrix was stained with Alizarin Red S on day 21. (A) Digital photos of different samples after staining with Alizarin Red S. (B) The production of mineralized matrix determined by quantifying the amount of Alizarin Red S that stained the mineralized matrix. Data were analyzed using one-way ANOVA against the osteoconductive group.

eventually attenuate the osteoblast response to DEX.[47] On the other hand, some positive regulators involved in the regulatory process of osteoblastic differentiation may be down-regulated by the high concentrations of DEX. Therefore, the decreased ALP activity for DEX@MSNs-pep at a concentration of 100 μg/mL was related to the effect of high concentrations of DEX. On the basis of the above finding, it is necessary to investigate the effects of different concentrations of MSNs-pep and DEX@MSNs-pep on ALP activity. Although the ALP activity increased with increasing content of BMP-2 peptide, it would cause negative effect at the presence of high DEX concentration. These results also suggested that the grafted peptide remained its biological activity after immobilized onto the surface of MSNs, and the incorporation of DEX could further enhance the upregulation of ALP activity.

3.5. In Vitro Mineralization. The mineralized matrix synthesis was assessed using an Alizarin Red S staining assay, which identifies calcium deposition, and the extent of calcium deposition was quantified by extracting the dye from the stained monolayer (Figure 8). After 21 days of differentiation, the BMSCs cultured in normal medium did not show any obvious calcium deposits (Figure 8A). Compared to BMSCs cultured in osteoductive medium, a significant increase in the amount of calcium deposition was observed when cells were

DOI: 10.1021/acsami.5b02636
ACS Appl. Mater. Interfaces 2015, 7, 15777−15789

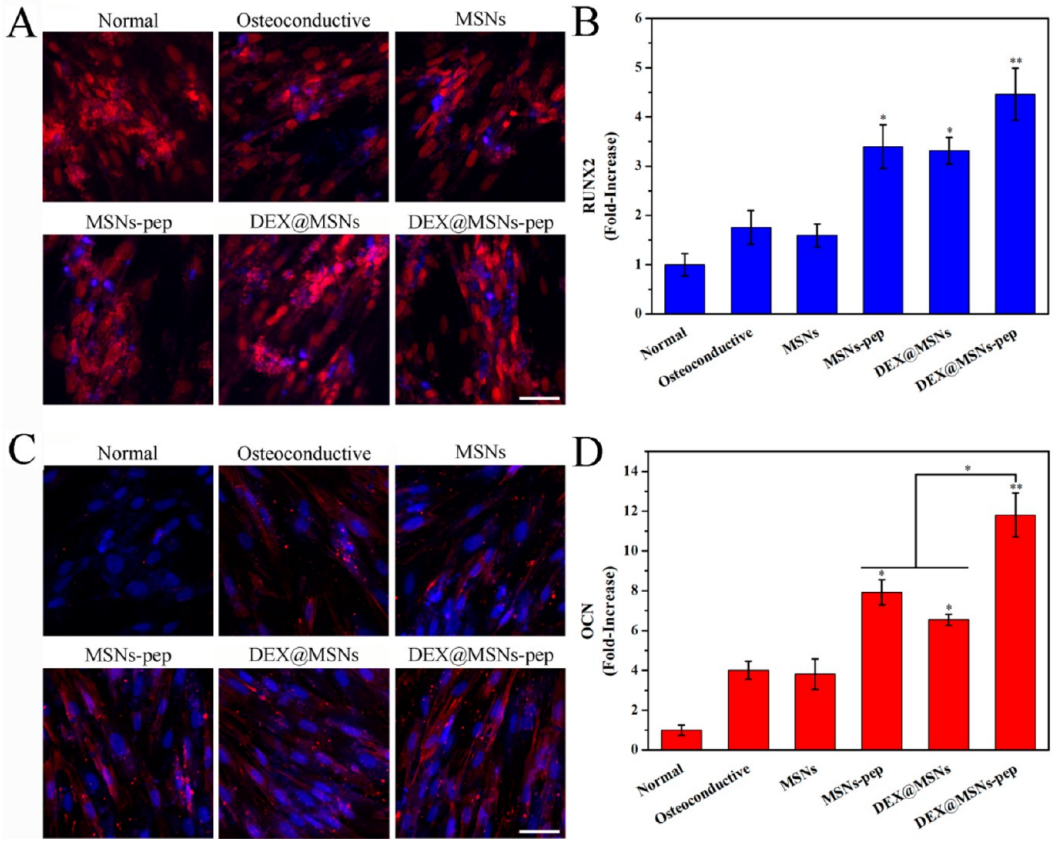

Figure 9. Immunostaining of osteo-related protein (A and C) and their quantitative analysis (B and D) on day 21. The expression of osteo-related proteins was quantified by using an Image-Pro Plus software analysis from the fluorescence images and normalized to the normal group. (A, blue) RUNX2 staining, cell nuclei were stained with (red) PI, and (B) quantitative analysis of RUNX2. (C) Osteocalcin (OCN, red) staining, cell nuclei were stained with DAPI (blue), and (D) quantitative analysis of OCN. Data were analyzed using one-way ANOVA against the osteoconductive group. Scale bar = 50 μm.

cultured with MSNs-pep, DEX@MSNs or DEX@MSNs-pep (Figure 8B). Remarkably, for the combination of BMP-2 peptide and DEX, cells cultured with DEX@MSNs-pep exhibited statistically significant increase in calcium deposition than those with MSNs-pep and DEX@MSNs ($P < 0.01$). These findings demonstrated that BMP-2 peptide grafted MSNs can promote the formation of mineralized matrix and further enhance the efficiency of mineralization after DEX loading.

3.6. Immunocytochemical Analysis. Among the evaluations of osteogenic differentiation, the characterizations of osteo-related proteins expression are equally important, like RUNX-related transcription factor 2 (RUNX2) and osteocalcin (OCN). RNUX2 belongs to the RUNX family of transcription factors and is one of the earliest indications of osteoblastic differentiation, which can stimulate the expression of key osteogenic genes such as OCN and osteopontin (OPN).[48−50] The expression level of RNUX2 at day 21 was shown in Figure 9A,B. Compared with normal medium, BMSCs cultured in osteoconductive medium and with the addition of materials showed the positive for RNUX2 protein. Stronger fluorescence intensity was observed for MSNs-pep, DEX@MSNs and DEX@MSNs-pep (Figure 9A), indicating that there were more RUNX2 protein expression. The result of quantified analysis also confirmed that the addition of MSNs-pep, DEX@MSNs or DEX@MSNs-pep significantly promotes RUNX2 expression (Figure 9B). In the BMP signaling pathway, RUNX2 is a critical transcription factor and is required for osteogenesis.[51] These nanoparticles containing BMP-2 peptide significantly enhanced the expression of RUNX2 protein compared to bare MSNs, which revealed that the BMP pathway was activated. We can rationally deduce that when BMP-2 peptide interacted with the BMP receptors on the cell surface, the formed complex could activate the downstream Smad pathway and then regulate gene expression of the osteogenic transcription factor, such as RUNX2.[52,53] However, it is unclear that how the peptide influence the osteogenic differentiation after uptake of nanoparticles by cells. These results are largely concordant with previous studies[28,51] showing that the BMP-2 peptide still kept its bioactivity after being incorporated onto the nanoparticles.

OCN is the bone-specific protein synthesized by osteoblasts and acts as a marker to evaluate osteogenic maturation and bone formation, which manifests the greatest expression at the late stage of osteogenesis.[54] Figure 9C shows the expression level of OCN marker at day 21. It was clearly visible that an enhanced fluorescence was observed in the MSNs-pep, DEX@MSNs and DEX@MSNs-pep groups, suggesting these bioactive nanoparticles could enhance the expression of OCN. In addition, the expression of OCN in DEX@MSNs-pep group was significantly higher ($P < 0.05$) than that in MSNs-pep and DEX@MSNs groups (Figure 9D).

3.7. Ectopic Bone Formation in Rats. The ectopic bone formation in vivo was used to further evaluate the osteogenic capacity of MSNs-pep and DEX@MSNs-pep. At 3 weeks postoperation, the bone formation in implanted region was analyzed by CT images (Figure 10). In the MSN group, no

DOI: 10.1021/acsami.5b02636
ACS Appl. Mater. Interfaces 2015, 7, 15777−15789

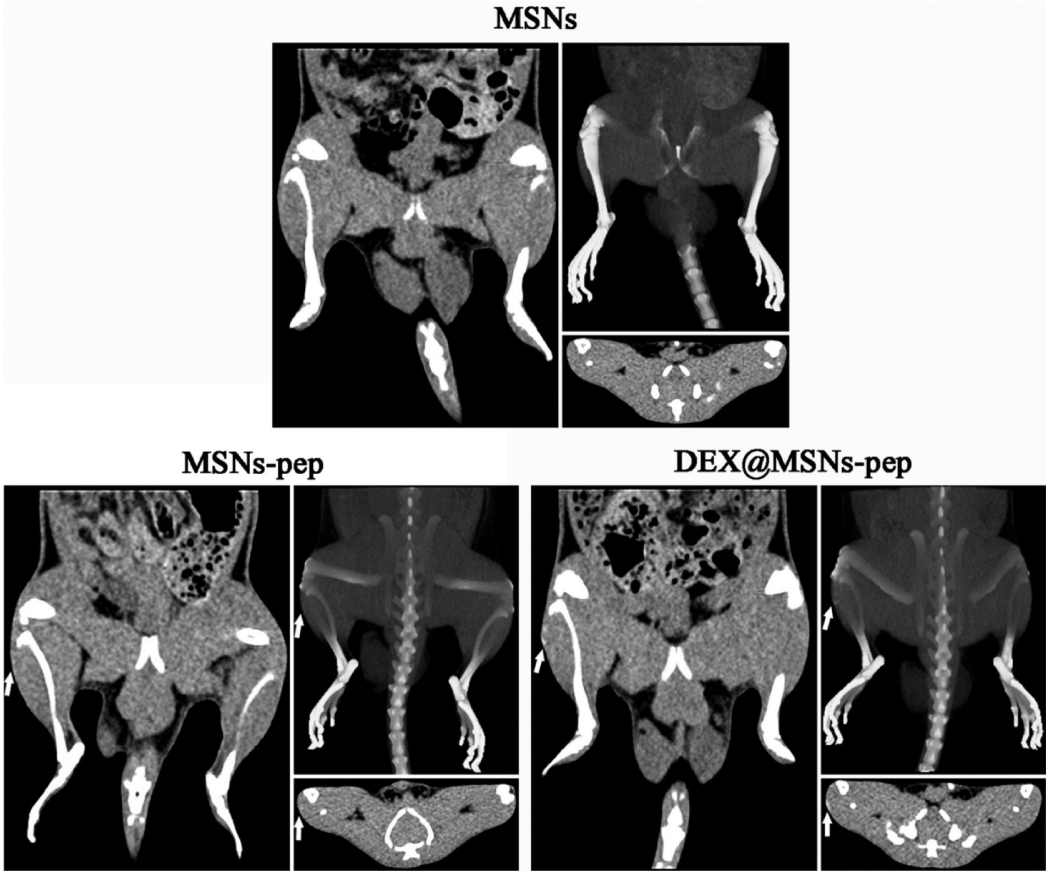

Figure 10. CT images of rats implanted with different implants for 3 weeks. Images of (left) plain CT scanning, (upper right) three-dimensional CT reconstruction, and (bottom right) transverse section for each MSNs, MSNs-pep, and DEX@MSNs-pep.

evident calcified deposits were observed in rat, but for both the MSNs-pep and DEX@MSNs-pep groups, the shadows (white arrow) generated by the calcification were emerged in the area surrounding the implanted regions. Furthermore, the CT images showed that the DEX@MSNs-pep group induced more obvious mineralization than the MSNs-pep group. In addition, HE staining was performed to confirm the ectopic bone formation (Figure 11). The histological observation showed

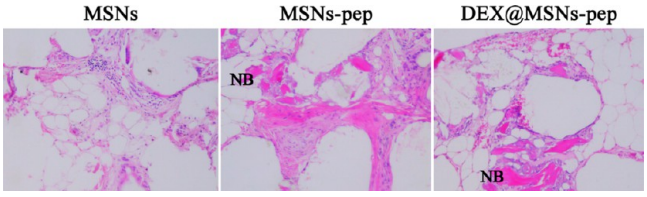

Figure 11. Histological evaluation with HE staining of ectopic bone formation at 3 weeks. NB, new bone; magnification, 100×.

that no obvious bone formation was observed in the MSNs group. In contrast, newly formed bone was found in the area of implanted regions for the MSNs-pep and DEX@MSNs-pep groups. It is noted that the amount of new bone in the DEXMSNs-pep group was greater than that of the MSNs-pep group. These results demonstrated that BMP-2 peptide incorporated MSNs hold the capacity of inducing ectopic bone formation in vivo, and this capacity can be strengthened in the presence of DEX. However, this constructed nanoparticulate osteogenic delivery systems did not seem to induce a robust osteogenic response. But we expect that they could be potentially applied in bone repair without causing adverse effects as BMP-2 protein did.

Previous studies reported that immobilization of BMP peptide in biomaterials could promote osteogenic differentiation of mesenchymal stem cells or preosteoblast.[6,28,29,39] However, the bone formation process is controlled sequentially and cooperatively by many growth factors.[55] To further enhance the osteogenic differentiation, other bioactive factor was frequently added to serve as a synergetic factor. In this study, DEX was loaded in the mesopores of BMP-2 peptide grafted MSNs and was released from the pores in a sustained manner, which supplied the sufficient amount of DEX to promote the differentiation of osteogenic cells without the extra addition of DEX in the culture medium. As a result, DEX release from MSNs-pep further promotes the osteogenic differentiation of BMSCs in terms of ALP activity, calcium deposition and osteo-related protein expression. On the basis of the above obtained results, a possible model to understand the effects of BMP-2 peptide and DEX on the osteogenic differentiation of BMSCs is proposed. As illustrated in Figure 12, the peptide grafting not only endows nanoparticles with good dispersibility and biocompatibility, but also enhances the cellular uptake due to the high affinity of BMP-2 peptide and specific BMP receptors and electrostatic adsorption of heterogeneous surface charge. Moreover, the BMP-2 peptide interacts with BMP receptors on the cell surface, which results in the formation of peptide/BMP receptors complexes and the activation of downstream Smad pathways.[56] After being taken

DOI: 10.1021/acsami.5b02636
ACS Appl. Mater. Interfaces 2015, 7, 15777−15789

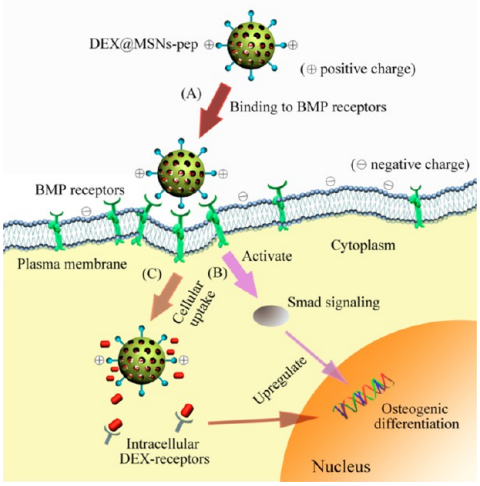

Figure 12. Schematic diagram of the influence of DEX@MSNs-pep on osteogenic differentiation. (A) DEX@MSNs-pep nanoparticles bind to the cells surface via the interaction with specific BMP receptors and electrostatic adsorption, thus forming the complexes. (B) The formation of complexes potentially activates the downstream osteogenic pathways. (C) DEX@MSNs-pep is delivered into cells by endocytosis, and DEX is released into cytoplasm. Finally, BMP-2 peptide and DEX stimulate and enhance the osteogenic differentiation together.

up by cells, DEX is released into the cytoplasm and then binds to its receptor. Consequently, the combination usage of bioactive BMP-2 peptide and DEX exerted a synergistic effect on the osteogenic differentiation of BMSCs.

4. CONCLUSION

In summary, the bioactive BMP-2 peptide grafted MSNs were synthesized by covalently conjugation of BMP-2 peptide and aminated MSNs. After BMP-2 peptide grafting, the dispersibility and biocompatibility of functionalized MSNs were improved, while the cellular uptake of nanoparticles against BMSCs was enhanced. The experimental results also showed that the prepared MSNs-pep promoted the osteogenic differentiation of BMSCs in vitro, as indicated by the upregulation of ALP activity and osteo-related proteins expression, as well as the increased calcium deposition. Moreover, the loading of DEX in MSNs-pep further enhanced the osteogenic differentiation of BMSCs. In addition, based on the results of CT images and histological examination, the DEX@MSNs-pep delivery system could induce significant ectopic bone formation in vivo. Therefore, the BMP-2 peptide and DEX-incorporated MSNs showed a higher capacity for osteogenic differentiation and hold great potential for bone tissue engineering applications.

■ ASSOCIATED CONTENT

Supporting Information

UV−vis spectra of MSNs-pep before and after centrifugation; photos of FITC-conjugated MSNs and MSNs-pep dispersed in different solutions; side-view from z-stack images of BMSCs incubated with different samples; in vitro cellular uptake of MSNs-pep and MSNs-pep with noggin against BMSCs; zeta potential of synthesized MSNs, MSNs-NH_2, and MSNs-pep; in vitro release curve of DEX from DEX@MSNs-pep in PBS solution (pH 7.4). The Supporting Information is available free of charge on the ACS Publications website at DOI: 10.1021/acsami.5b02636.

■ AUTHOR INFORMATION

Corresponding Author

*Tel./Fax: +86 21 6779 2742. E-mail: hcl@dhu.edu.cn.

Notes

The authors declare no competing financial interest.

■ ACKNOWLEDGMENTS

This study was financially supported by the National Natural Science Foundation of China (31271028), Innovation Program of Shanghai Municipal Education Commission (13ZZ051), Open Foundation of State Key Laboratory for Modication of Chemical Fibers and Polymer Materials (LK1416) and Chinese Universities Scientific Fund (CUSF-DH-D-2014019).

■ REFERENCES

(1) Bolland, B. J.; Partridge, K.; Tilley, S.; New, A. M.; Dunlop, D. G.; Oreffo, R. O. Biological and Mechanical Enhancement of Impacted Allograft Seeded with Human Bone Marrow Stromal Cells: Potential Clinical Role in Impaction Bone Grafting. *Regener. Med.* **2006**, *1*, 457−467.

(2) Reichert, J. C.; Epari, D. R.; Wullschleger, M. E.; Saifzadeh, S.; Steck, R.; Lienau, J.; Sommerville, S.; Dickinson, I. C.; Schütz, M. A.; Duda, G. N. Establishment of a Preclinical Ovine Model for Tibial Segmental Bone Defect Repair by Applying Bone Tissue Engineering Strategies. *Tissue Eng., Part B* **2010**, *16*, 93−104.

(3) He, C. L.; Zhang, F.; Cao, L. J.; Feng, W.; Qiu, K. X.; Zhang, Y. Z.; Wang, H. S.; Mo, X. M.; Wang, J. W. Rapid Mineralization of Porous Gelatin Scaffolds by Electrodeposition for Bone Tissue Engineering. *J. Mater. Chem.* **2012**, *22*, 2111−2119.

(4) Vines, J. B.; Lim, D.-J.; Anderson, J. M.; Jun, H.-W. Hydroxyapatite Nanoparticle Reinforced Peptide Amphiphile Nanomatrix Enhances the Osteogenic Differentiation of Mesenchymal Stem Cells by Compositional Ratios. *Acta Biomater.* **2012**, *8*, 4053−4063.

(5) He, C. L.; Jin, X. B.; Ma, P. X. Calcium Phosphate Deposition Rate, Structure and Osteoconductivity on Electrospun Poly(L-Lactic Acid) Matrix Using Electrodeposition or Simulated Body Fluid Incubation. *Acta Biomater.* **2014**, *10*, 419−427.

(6) Przybylowski, C.; Quinn, T.; Callahan, A.; Kaplan, M.; Golding, A.; Alesi, C.; Ammar, M.; LeBlon, C. E.; Guo, Y.; Zhang, X. MC3T3 Preosteoblast Differentiation on Bone Morphogenetic Protein-2 Peptide Ormosils. *J. Mater. Chem.* **2012**, *22*, 10672−10683.

(7) Ravichandran, R.; Gandhi, S.; Sundaramurthi, D.; Sethuraman, S.; Krishnan, U. M. Hierarchical Mesoporous Silica Nanofibers as Multifunctional Scaffolds for Bone Tissue Regeneration. *J. Biomater. Sci., Polym. Ed.* **2013**, *24*, 1988−2005.

(8) Zhou, H.; Wu, X.; Wei, J.; Lu, X.; Zhang, S.; Shi, J.; Liu, C. Stimulated Osteoblastic Proliferation by Mesoporous Silica Xerogel with High Specific Surface Area. *J. Mater. Sci.: Mater. Med.* **2011**, *22*, 731−739.

(9) Feng, W.; Zhou, X.; He, C.; Qiu, K.; Nie, W.; Chen, L.; Wang, H.; Mo, X.; Zhang, Y. Polyelectrolyte Multilayer Functionalized Mesoporous Silica Nanoparticles for pH-Responsive Drug Delivery: Layer Thickness-Dependent Release Profiles and Biocompatibility. *J. Mater. Chem. B* **2013**, *1*, 5886−5898.

(10) Slowing, I. I.; Vivero-Escoto, J. L.; Wu, C.-W.; Lin, V. S.-Y. Mesoporous Silica Nanoparticles as Controlled Release Drug Delivery and Gene Transfection Carriers. *Adv. Drug Delivery Rev.* **2008**, *60*, 1278−1288.

(11) Qiu, K.; He, C.; Feng, W.; Wang, W.; Zhou, X.; Yin, Z.; Chen, L.; Wang, H.; Mo, X. Doxorubicin-Loaded Electrospun Poly (L-Lactic Acid)/Mesoporous Silica Nanoparticles Composite Nanofibers for Potential Postsurgical Cancer Treatment. *J. Mater. Chem. B* **2013**, *1*, 4601−4611.

DOI: 10.1021/acsami.5b02636
ACS Appl. Mater. Interfaces 2015, 7, 15777−15789

(12) Feng, W.; Nie, W.; He, C.; Zhou, X.; Chen, L.; Qiu, K.; Wang, W.; Yin, Z. Effect of pH-Responsive Alginate/Chitosan Multilayers Coating on Delivery Efficiency, Cellular Uptake and Biodistribution of Mesoporous Silica Nanoparticles Based Nanocarriers. *ACS Appl. Mater. Interfaces* **2014**, *6*, 8447−8460.
(13) Slowing, I. I.; Trewyn, B. G.; Giri, S.; Lin, V. Y. Mesoporous Silica Nanoparticles for Drug Delivery and Biosensing Applications. *Adv. Funct. Mater.* **2007**, *17*, 1225−1236.
(14) He, C. L.; Nie, W.; Feng, W. Engineering of Biomimetic Nanofibrous Matrices for Drug Delivery and Tissue Engineering. *J. Mater. Chem. B* **2014**, *2*, 7828−7848.
(15) He, C. L.; Xiao, G. Y.; Jin, X. B.; Sun, C. H.; Ma, P. X. Electrodeposition on Nanofibrous Polymer Scaffolds: Rapid Mineralization, Tunable Calcium Phosphate Composition and Topography. *Adv. Funct. Mater.* **2010**, *20*, 3568−3576.
(16) Tautzenberger, A.; Kovtun, A.; Ignatius, A. Nanoparticles and Their Potential for Application in Bone. *Int. J. Nanomed.* **2012**, *7*, 4545−4557.
(17) Cho, H.-j.; Madhurakkat Perikamana, S. K.; Lee, J.-h.; Lee, J.; Lee, K.-M.; Shin, C. S.; Shin, H. Effective Immobilization of BMP-2 Mediated by Polydopamine Coating on Biodegradable Nanofibers for Enhanced in Vivo Bone Formation. *ACS Appl. Mater. Interfaces* **2014**, *6*, 11225−11235.
(18) Su, Y.; Su, Q.; Liu, W.; Lim, M.; Venugopal, J. R.; Mo, X.; Ramakrishna, S.; Al-Deyab, S. S.; El-Newehy, M. Controlled Release of Bone Morphogenetic Protein 2 and Dexamethasone Loaded in Core-Shell PLLACL-Collagen Fibers for Use in Bone Tissue Engineering. *Acta Biomater.* **2012**, *8*, 763−771.
(19) Hu, Y.; Cai, K. Y.; Luo, Z.; Jandt, K. D. Layer-by-Layer Assembly of β-Estradiol Loaded Mesoporous Silica Nanoparticles on Titanium Substrates and Its Implication for Bone Homeostasis. *Adv. Mater.* **2010**, *22*, 4146−4150.
(20) David, L.; Feige, J.-J.; Bailly, S. Emerging Role of Bone Morphogenetic Proteins in Angiogenesis. *Cytokine Growth Factor Rev.* **2009**, *20*, 203−212.
(21) Yasko, A. W.; Lane, J.; Fellinger, E.; Rosen, V.; Wozney, J.; Wang, E. The Healing of Segmental Bone Defects, Induced by Recombinant Human Bone Morphogenetic Protein (rhBMP-2). A Radiographic, Histological, and Biomechanical Study in Rats. *J. Bone Jt. Surg. Am. Vol.* **1992**, *74*, 659−670.
(22) Shimer, A. L.; Öner, F. C.; Vaccaro, A. R. Spinal Reconstruction and Bone Morphogenetic Proteins: Open Questions. *Injury* **2009**, *40*, S32−S38.
(23) Chung, Y.-I.; Ahn, K.-M.; Jeon, S.-H.; Lee, S.-Y.; Lee, J.-H.; Tae, G. Enhanced Bone Regeneration with BMP-2 Loaded Functional Nanoparticle-Hydrogel Complex. *J. Controlled Release* **2007**, *121*, 91−99.
(24) Chen, F. M.; Wu, Z. F.; Sun, H. H.; Wu, H.; Xin, S. N.; Wang, Q. T.; Dong, G. Y.; Ma, Z. W.; Huang, S.; Zhang, Y. J. Release of Bioactive Bmp from Dextran-Derived Microspheres: A Novel Delivery Concept. *Int. J. Pharm.* **2006**, *307*, 23−32.
(25) Xie, G.; Sun, J.; Zhong, G.; Liu, C.; Wei, J. Hydroxyapatite Nanoparticles as a Controlled-Release Carrier of BMP-2: Absorption and Release Kinetics *in Vitro*. *J. Mater. Sci.: Mater. Med.* **2010**, *21*, 1875−1880.
(26) Neumann, A.; Christel, A.; Kasper, C.; Behrens, P. BMP2-Loaded Nanoporous Silica Nanoparticles Promote Osteogenic Differentiation of Human Mesenchymal Stem Cells. *RSC Adv.* **2013**, *3*, 24222−24230.
(27) Gan, Q.; Zhu, J.; Yuan, Y.; Liu, H.; Qian, J.; Li, Y.; Liu, C. A Dual-Delivery System of pH-Responsive Chitosan-Functionalized Mesoporous Silica Nanoparticles Bearing BMP-2 and Dexamethasone for Enhanced Bone Regeneration. *J. Mater. Chem. B* **2015**, *3*, 2056−2066.
(28) Sun, Y.; Deng, Y.; Ye, Z.; Liang, S.; Tang, Z.; Wei, S. Peptide Decorated Nano-Hydroxyapatite with Enhanced Bioactivity and Osteogenic Differentiation *Via* Polydopamine Coating. *Colloids Surf., B* **2013**, *111*, 107−116.
(29) Kim, Y.; Renner, J. N.; Liu, J. C. Incorporating the BMP-2 Peptide in Genetically-Engineered Biomaterials Accelerates Osteogenic Differentiation. *Biomater. Sci.* **2014**, *2*, 1110−1119.
(30) Saito, A.; Suzuki, Y.; Ogata, S.-i.; Ohtsuki, C.; Tanihara, M. Activation of Osteo-Progenitor Cells by a Novel Synthetic Peptide Derived from the Bone Morphogenetic Protein-2 Knuckle Epitope. *Biochim. Biophys. Acta, Proteins Proteomics* **2003**, *1651*, 60−67.
(31) Saito, A.; Suzuki, Y.; Ogata, S. I.; Ohtsuki, C.; Tanihara, M. Prolonged Ectopic Calcification Induced by BMP-2-Derived Synthetic Peptide. *J. Biomed. Mater. Res.* **2004**, *70*, 115−121.
(32) He, X.; Ma, J.; Jabbari, E. Effect of Grafting RGD and BMP-2 Protein-Derived Peptides to a Hydrogel Substrate on Osteogenic Differentiation of Marrow Stromal Cells. *Langmuir* **2008**, *24*, 12508−12516.
(33) Saito, A.; Suzuki, Y.; Kitamura, M.; Ogata, S. I.; Yoshihara, Y.; Masuda, S.; Ohtsuki, C.; Tanihara, M. Repair of 20-Mm Long Rabbit Radial Bone Defects Using BMP-Derived Peptide Combined with an α-Tricalcium Phosphate Scaffold. *J. Biomed. Mater. Res., Part A* **2006**, *77*, 700−706.
(34) Lu, Y.; Lee, J. S.; Nemke, B.; Graf, B. K.; Royalty, K.; Illgen, R., III; Vanderby, R., Jr; Markel, M. D.; Murphy, W. L. Coating with a Modular Bone Morphogenetic Peptide Promotes Healing of a Bone-Implant Gap in an Ovine Model. *PLoS One* **2012**, *7*, e50378.
(35) Kim, H. K.; Kim, J. H.; Park, D. S.; Park, K. S.; Kang, S. S.; Lee, J. S.; Jeong, M. H.; Yoon, T. R. Osteogenesis Induced by a Bone Forming Peptide from the Prodomain Region of BMP-7. *Biomaterials* **2012**, *33*, 7057−7063.
(36) Radu, D. R.; Lai, C.-Y.; Jeftinija, K.; Rowe, E. W.; Jeftinija, S.; Lin, V. S.-Y. A Polyamidoamine Dendrimer-Capped Mesoporous Silica Nanosphere-Based Gene Transfection Reagent. *J. Am. Chem. Soc.* **2004**, *126*, 13216−13217.
(37) Pan, L.; He, Q.; Liu, J.; Chen, Y.; Ma, M.; Zhang, L.; Shi, J. Nuclear-Targeted Drug Delivery of TAT Peptide-Conjugated Monodisperse Mesoporous Silica Nanoparticles. *J. Am. Chem. Soc.* **2012**, *134*, 5722−5725.
(38) Kim, K. S.; Lee, J. Y.; Kang, Y. M.; Kim, E.; Kim, G. H.; Rhee, S. D.; Cheon, H. G.; Kim, J. H.; Min, B.-H.; Lee, H. B. Small Intestine Submucosa Sponge for *in Vivo* Support of Tissue-Engineered Bone Formation in the Presence of Rat Bone Marrow Stem Cells. *Biomaterials* **2010**, *31*, 1104−1113.
(39) Zouani, O. F.; Chollet, C.; Guillotin, B.; Durrieu, M.-C. Differentiation of Pre-Osteoblast Cells on Poly (Ethylene Terephthalate) Grafted with RGD and/or BMPs Mimetic Peptides. *Biomaterials* **2010**, *31*, 8245−8253.
(40) Du, L.; Song, H. Y.; Liao, S. J. A Biocompatible Drug Delivery Nanovalve System on the Surface of Mesoporous Nanoparticles. *Microporous Mesoporous Mater.* **2012**, *147*, 200−204.
(41) Zhou, X.; Cheng, X.; Feng, W.; Qiu, K.; Chen, L.; Nie, W.; Yin, Z.; Mo, X.; Wang, H.; He, C. Synthesis of Hollow Mesoporous Silica Nanoparticles with Tunable Shell Thickness and Pore Size Using Amphiphilic Block Copolymers as Core Templates. *Dalton Trans.* **2014**, *43*, 11834−11842.
(42) Wang, Y.; Shi, W.; Song, W.; Wang, L.; Liu, X.; Chen, J.; Huang, R. Tumor Cell Targeted Delivery by Specific Peptide-Modified Mesoporous Silica Nanoparticles. *J. Mater. Chem.* **2012**, *22*, 14608−14616.
(43) Chen, Y.; Chen, H.; Zeng, D.; Tian, Y.; Chen, F.; Feng, J.; Shi, J. Core/Shell Structured Hollow Mesoporous Nanocapsules: A Potential Platform for Simultaneous Cell Imaging and Anticancer Drug Delivery. *ACS Nano* **2010**, *4*, 6001−6013.
(44) Krause, C.; Guzman, A.; Knaus, P. Noggin. *Int. J. Biochem. Cell Biol.* **2011**, *43*, 478−481.
(45) Lima, A. C.; Puga, A. M.; Mano, J. F.; Concheiro, A.; Alvarez-Lorenzo, C. Free and Copolymerized γ-Cyclodextrins Regulate Performance of Dexamethasone-Loaded Dextran Microspheres for Bone Regeneration. *J. Mater. Chem. B* **2014**, *2*, 4943−4956.
(46) Pittenger, M. F.; Mackay, A. M.; Beck, S. C.; Jaiswal, R. K.; Douglas, R.; Mosca, J. D.; Moorman, M. A.; Simonetti, D. W.; Craig,

DOI: 10.1021/acsami.5b02636
ACS Appl. Mater. Interfaces 2015, 7, 15777−15789

S.; Marshak, D. R. Multilineage Potential of Adult Human Mesenchymal Stem Cells. *Science* **1999**, *284*, 143−147.
(47) Ishida, Y.; Heersche, J. N. M. Glucocorticoid-Induced Osteoporosis: Both in Vivo and in Vitro Concentrations of Glucocorticoids Higher Than Physiological Levels Attenuate Osteoblast Differentiation. *J. Bone Miner. Res.* **1998**, *13*, 1822−1826.
(48) Ducy, P.; Schinke, T.; Karsenty, G. The Osteoblast: A Sophisticated Fibroblast under Central Surveillance. *Science* **2000**, *289*, 1501−1504.
(49) Bae, S.-C.; Lee, Y. H. Phosphorylation, Acetylation and Ubiquitination: The Molecular Basis of Runx Regulation. *Gene* **2006**, *366*, 58−66.
(50) Centrella, M.; Christakos, S.; McCarthy, T. L. Skeletal Hormones and the C/EBP and Runx Transcription Factors: Interactions That Integrate and Redefine Gene Expression. *Gene* **2004**, *342*, 13−24.
(51) Mercado, A. E.; Yang, X.; He, X.; Jabbari, E. Effect of Grafting BMP2-Derived Peptide to Nanoparticles on Osteogenic and Vasculogenic Expression of Stromal Cells. *J. Tissue Eng. Regener. Med.* **2014**, *8*, 15−28.
(52) Langenbach, F.; Handschel, J. Effects of Dexamethasone, Ascorbic Acid and β-Glycerophosphate on the Osteogenic Differentiation of Stem Cells in Vitro. *Stem Cell Res. Ther.* **2013**, *4*, 117.
(53) Chen, D.; Zhao, M.; Mundy, G. R. Bone Morphogenetic Proteins. *Growth Factors* **2004**, *22*, 233−41.
(54) Ducy, P.; Desbois, C.; Boyce, B.; Pinero, G.; Story, B.; Dunstan, C.; Smith, E.; Bonadio, J.; Goldstein, S.; Gundberg, C. Increased Bone Formation in Osteocalcin-Deficient Mice. *Nature* **1996**, *382*, 448−452.
(55) Hanada, K.; Dennis, J. E.; Caplan, A. I. Stimulatory Effects of Basic Fibroblast Growth Factor and Bone Morphogenetic Protein-2 on Osteogenic Differentiation of Rat Bone Marrow-Derived Mesenchymal Stem Cells. *J. Bone Miner. Res.* **1997**, *12*, 1606−1614.
(56) Miyazono, K. Signal Transduction by Bone Morphogenetic Protein Receptors: Functional Roles of SMAD Proteins. *Bone* **1999**, *25*, 91−93.

DOI: 10.1021/acsami.5b02636
ACS Appl. Mater. Interfaces 2015, 7, 15777−15789